Eur. Phys. J. E **27**, 205–211 (2008)
DOI 10.1140/epje/i2008-10373-8

THE EUROPEAN PHYSICAL JOURNAL E

Aggregation of a hydrophobically modified poly(propylene imine) dendrimer

Susheng Tan[1,a], Aihua Su[2,b], and Warren T. Ford[2,c]

[1] Microscopy Laboratory, Oklahoma State University, 1110 S Innovation Way, Stillwater, OK 74074, USA
[2] Department of Chemistry, Oklahoma State University, Stillwater, OK 74078, USA

Received 26 February 2008 and Received in final form 23 June 2008
Published online: 16 October 2008 –

Abstract. The poly(propylene imine) dendrimer DAB-dendr-$(NH_2)_8$ was hydrophobically modified with dodecanoyl end groups. The modified dendrimer was deposited onto mica by adsorption from solution and observed by atomic force microscopy. With the decrease of adsorption time, the modified dendrimer varied from continuous film to scattered islands. For the adsorption time of 20 s the dendrimer formed a sub-monolayer thin film that contained many fractal aggregates of fractal dimension 1.80 that were $> 1\,\mu$m in diameter and no more than 0.8 nm thick. After 5 months at 25 °C, the initial fractal aggregates transformed into disks and other less-branched shapes with average heights of the domains of 0.6 nm and 0.4 nm, respectively. Formation of the fractal aggregates is explained by diffusion-limited aggregation. The slow reorganization of dendrimer molecules in the fractal aggregates occurs at a temperature well above the T_g of the dendrimer.

PACS. 68.47.Pe Langmuir-Blodgett films on solids; polymers on surfaces; biological molecules on surfaces – 61.43.Hv Fractals; macroscopic aggregates (including diffusion-limited aggregates) – 68.37.Ps Atomic force microscopy (AFM)

1 Introduction

Dendritic macromolecules have regular repeating chain segments between branch points that reach out from a central core [1,2]. They have potential applications in electrical, optical, and opto-electrical devices. Recent review articles present us the excellent standing status of dendrimer research and development [2–5]. Dendrimers have variable interactions with interfaces depending on their surface properties. Their adsorption at the air-liquid interface or at the liquid-solid interface has suggested that electrostatic interactions play a negligible role and that PPI and PAMAM dendrimers behave similarly. Adsorption of PAMAM dendrimers, particularly of higher generations, studied by atomic force microscopy (AFM) revealed that such dendrimers flatten substantially upon adsorption. Spin-cast samples of carbosilane dendrimers have been shown to pseudopartially wet the mica interface, yielding a 1.4 nm thick monolayer of adsorbed dendrimer interspersed with macroscopic droplets of bulk carbosilane [6]. Amphiphilic dendrimers can self-assemble on solid substrates and at the air-water interface [7–9]. Langmuir-Blodgett films of poly(propylene imine) dendrimers are ordered monolayers, at least at low surface pressures [9]. Meijer and coworkers modified end groups of PPI (poly(propylene imine)) dendrimers using long hydrophobic chains [10,11] and found that the conformational flexibility of dendrimer branches allows for the folding of the dendritic structure and formation of a pancake shape of the polar cores at the air-water interface. The hydrophobically modified dendrimers form monolayers at the air/water interface with the hydrophilic core in contact with the water subphase and the hydrophobic end groups extending perpendicularly away from the water surface in contact with air. The results for PPI dendrimers are in agreement with findings on deuterated poly(benzyl ether) dendrons [12,13], end-grafted poly(amido amine) dendrimers [14–16], and hydrophobically modified hyperbranched polyesters [17–20]. In general, the adsorption and the resulting organization of dendrimers at interfaces have only received modest attention.

An amphiphilic monolayer can markedly alter the properties of an interface between two solids. For example an alkyl poly(ethylene glycol) stabilizes passivation at the interface of the electrode and the poly(ethylene oxide) (PEO) electrolyte of a solid-state lithium ion battery [21]. We reason that hydrophobically modified dendrimers may

[a] e-mail: susheng.tan@okstate.edu
[b] *Present address:* Food & Agricultural Product Research and Technology Center, Stillwater, OK 74078, USA.
[c] e-mail: warren.ford@okstate.edu

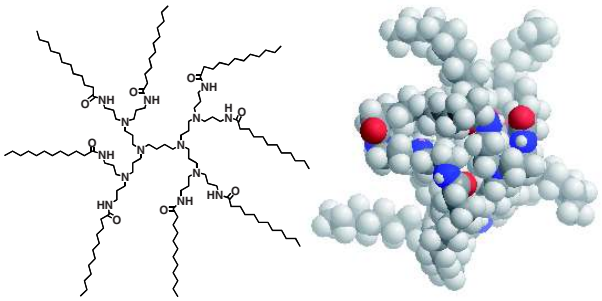

1

Fig. 1. Structure of dendrimer **1** and an energy-minimized (MM2) space-filling conformation [23]. The dendrimer has a pseudo two-dimensional shape with a relative shape anisotropy of 0.22 (0 for high three-dimensional symmetry, 0.25 for planar arrays, and 1.0 for a linear array of atoms) [24,25].

have the same effect. The ability to precisely tailor the chemistry of dendrimers so as to regulate their interaction with each other and the substrate is a great advantage of these systems. The problem of dendrimer organization during film casting on a substrate is of fundamental interest as well as is important to progress in technological applications [22]. In preparation for deposition of monolayers of the dendrimers onto PEO, we are investigating their monolayers at interfaces of air with solids and with water. Thus, understanding how these interfacial films form is needed. Here we report our observations on the morphology of adsorbed aggregates of a poly(propylene imine) (PPI) DAB-dendr-$(NH_2)_8$ dendrimer that is hydrophobically modified with dodecanamide end groups (**1**) as shown in Figure 1.

Interestingly dendrimer **1** formed two-dimensional fractal aggregates at a very short adsorption time. Fractal aggregates are widely seen in sputter-deposited semiconductor films [26,27], electrochemically deposited conductive polymer films [28,29], and self-assembled monolayers [30] as well as peptide films [31,32]. The fractal phenomenon is also observed at certain interfaces of microphase–separated polymer blends [33,34]. The molecular structure of a dendrimer itself is fractal [35,36]. It would be interesting to know whether the fractal structure of the molecules can facilitate the formation of much larger fractal aggregates.

2 Experimental setup

2.1 Chemicals and instruments

DAB-dendr-$(NH_2)_8$ (PPI) and dodecanoyl chloride were purchased from Aldrich Chemical Co. Anhydrous *N*, *N*-dimethylformamide (DMF) and anhydrous triethylamine (TEA) were purchased from Acros Organics. All chemicals were used as received unless otherwise stated. The water used for synthetic experiments was purified on a Barnstead 3-column e-pure system to a conductivity of < 4 Mohm^{-1} cm^{-1}. MALDI-TOF mass spectra were carried out on a Voyager-DE PRO instrument using DHB (2,5-dihydroxybenzoic acid) and IAA (*trans*-3-indoleacrylic acid) as matrices. Dynamic light scattering (Malvern Instruments particle size analyzer, HPPS3.3) was used to measure the hydrodynamic diameter for the modified dendrimer in chloroform solution.

2.2 Dodecanoyl-modified dendrimer (1)

By the method of Pan [37], dodecanoyl chloride (2.63 g, 12.02 mmol) was added to 773 mg (1.00 mmol) DAB-dendr-$(NH_2)_8$, 3.0 mL of anhydrous DMF, and 2.1 mL (1.51 g, 15 mmol) of anhydrous triethylamine (TEA) in a 100 mL three-neck round bottom flask under nitrogen at 0 °C. After 10 min the solution was heated and stirred under nitrogen at 70 °C for 24 h. The mixture was cooled to 25 °C, 2.0 mL of water was added, the water and the dendrimer paste were mixed well using a spatula, and 20 mL of CH_2Cl_2 was added. The CH_2Cl_2 solution was washed with 1% aqueous K_2CO_3 (15 mL × 2) and saturated NaCl solution (1 × 15 mL). The CH_2Cl_2 was dried over anhydrous K_2CO_3 (3.0 g) and filtered by gravity. The CH_2Cl_2 was removed by rotary evaporation. The residue was dissolved in toluene (10 mL × 3), and toluene was removed by vacuum rotary evaporation. The product was dried under vacuum at 60 °C for 24 h to recover 1.504 g (85%) of a yellow sticky ointment. ^{1}H NMR (300 MHz, $CDCl_3$): δ, ppm = 0.88 (t, CH_3), 1.25 (m, CH_2), 1.62 (m, NCH$_2$CH_2CH$_2$NCO, NCH$_2$CH_2CH$_2$N, NCH$_2$CH_2CH_2CH$_2$N), 2.18 (t, NHCOCH_2), 2.40 (m, CH$_2$N(CH_2)$_2$, NCH_2CH$_2$CH$_2$CH_2N), 3.26 (q, CH_2NHCO), 6.97 (br, NHCO). ^{13}C NMR ($CDCl_3$, δ): 14.04 (alkyl *C*1), 22.64 (alkyl *C*2), 29.43-29.62 (alkyl *C*4-*C*8), 25.78 (NCH$_2$*C*H$_2$CH$_2$NH, NCH$_2$*C*H$_2$*C*H$_2$CH$_2$N), 25.91 (NCH$_2$*C*H$_2$CH$_2$NHCO), 31.85 (alkyl *C*3), 36.64 (alkyl *C*11), 37.77 (NCH$_2$CH$_2$*C*H$_2$NHCO), 51.41 (N*C*H$_2$CH$_2$CH$_2$NHCO), 51.94 (N*C*H$_2$CH$_2$*C*H$_2$N, NCH$_2$CH$_2$CH$_2$*C*H$_2$N), 173.64 (*C*=O). Calcd MW: 2229. MALDI-TOF MS, found: 2232.

2.3 Sample preparation for AFM measurements

Dendrimer aggregation on mica surface was achieved by physical adsorption. The dendrimer solution of 2.0 mg/mL in chloroform was applied to cover all of the newly cleaved mica surface with a hemisphere of solution followed by spin-coating at 2000 rpm for 2 min after adsorption for 20, 30, 60, and 120 s, respectively. The sample dried further at ambient conditions. All samples were examined by AFM within 48 h of preparation. For the samples with fractal aggregates, further AFM observation was conducted after 5 months.

2.4 AFM measurements

AFM images were collected using a Multimode Scanning Probe Microscope with Nanoscope IIIa controller (Digital Instruments, Santa Barbara, CA) in a tapping mode at

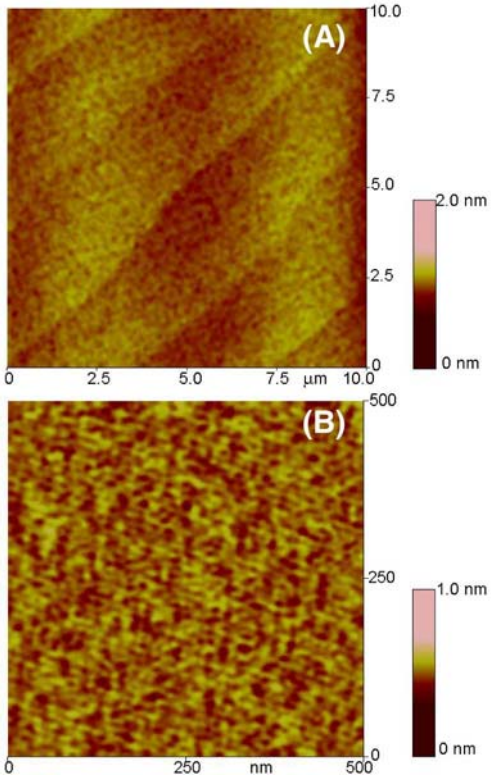

Fig. 2. AFM height images of dendrimer film on mica after 2 minutes adsorption. (B) is an enlarged scan at an area of (A).

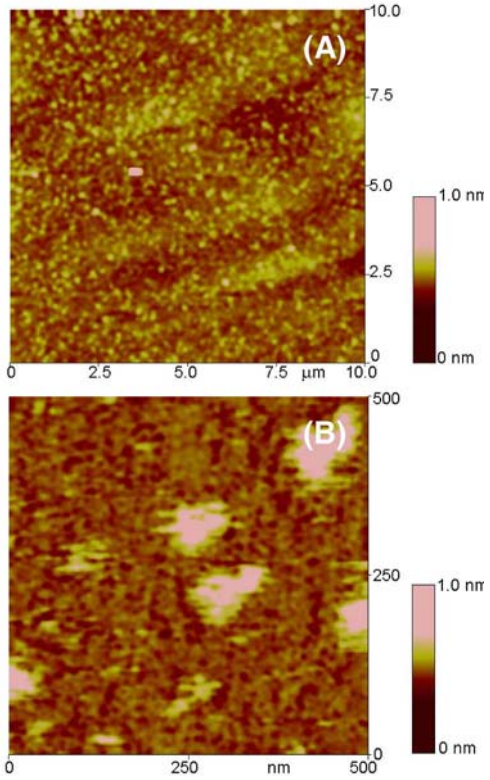

Fig. 3. AFM height images of dendrimer film on mica after 1 minute adsorption. (B) is an enlarged scan at an area of (A).

the set point ratio of 0.9 and a scanning rate of 1.0 Hz. The silicon probes (MikroMasch, Portland, Oregon) had a spring constant of 2–5 N/m, a resonance frequency of 120–170 kHz, and a nominal tip radius of curvature of 5–10 nm.

3 Results and discussion

3.1 Adsorption of dendrimer 1 on mica

To understand the kinetics of organization of the hydrophobically modified PPI dendrimers, we deposited the diluted dendrimer solution in chloroform on newly cleaved mica substrate and observed the morphologies of aggregate states of the dendrimers after varied adsorption times. The dendrimer formed a smooth, continuous film when the adsorption was allowed for 2 minutes, as shown in Figure 2. The root mean square roughness, R_{rms}, of areas of $10 \times 10\,\mu\mathrm{m}^2$ and $0.5 \times 0.5\,\mu\mathrm{m}^2$ was 0.11 nm and 0.08 nm, respectively. When the adsorption time was decreased to 1 minute, a mottled surface morphology was observed as shown in Figure 3. The R_{rms} values of areas of $10 \times 10\,\mu\mathrm{m}^2$ and $0.5 \times 0.5\,\mu\mathrm{m}^2$ were 0.16 and 0.14 nm, respectively. Protruding domains up to about 100 nm in size were observed at the surface. In terms of height the surface of the dendrimer adsorbed for 1 minute was heterogeneous. The phase images of the dendrimer films adsorbed on mica for 1 and 2 minutes were very uniform and showed phase shifts different from that of bare mica, which indicates full coverage of the mica surface by the dendrimer. Island domains of the modified PPI dendrimer were observed on mica when the adsorption time was further reduced to 0.5 minute, as shown in Figure 4. The sizes of the large domains varied from 1 μm to 2.5 μm. Also small domains surrounded the bigger islands. The heights of both the small domains and the big domains were very uniform and only about 0.8 nm. The islands exhibited a larger phase shift than the surrounding area and the newly cleaved mica. Thus there was less than a monolayer coverage of the dendrimer on mica.

Although we could not track the dendrimer aggregation at the solution-substrate interface in real time, these observations indicate that once one dendrimer molecule adsorbed to the mica, subsequent molecules adsorbed in contact with both mica and a previously adsorbed dendrimer. The dendrimer islands grew laterally rather than vertically, so that over time a complete continuous film developed [38, 39]. Growth of dendrimer aggregates at the mica surface is determined by the interfacial diffusion of dendrimer molecules to the solution-substrate interface. The evaporating solvent must be replenished from the liquid phase below. Therefore, there is a net flux of solvent away from and dendrimers towards the solution-substrate interface. Dendrimer-dendrimer attraction and weaker dendrimer-substrate attraction facilitate the formation of small islands. Dendrimer molecules and small aggregates diffuse and stick to the island perimeter or are integrated into the interior of an island by diffusing across

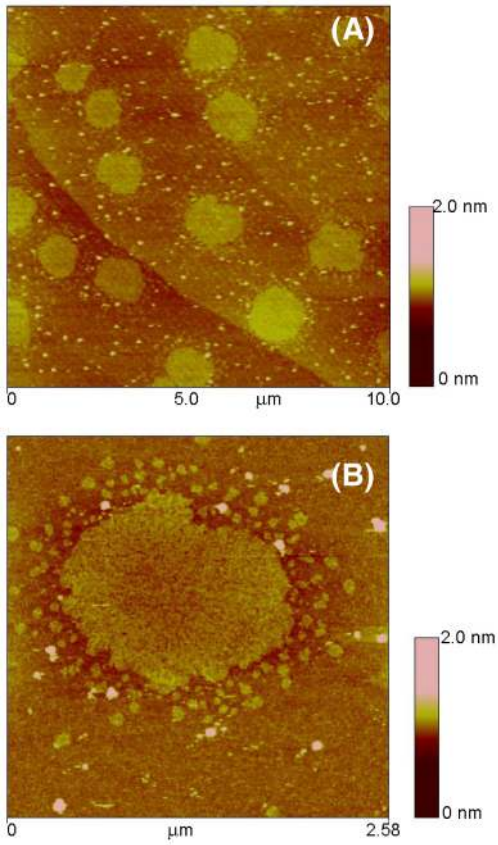

Fig. 4. AFM height images of dendrimer film on mica after 0.5 minute adsorption. (B) is an enlarged scan at an area of (A).

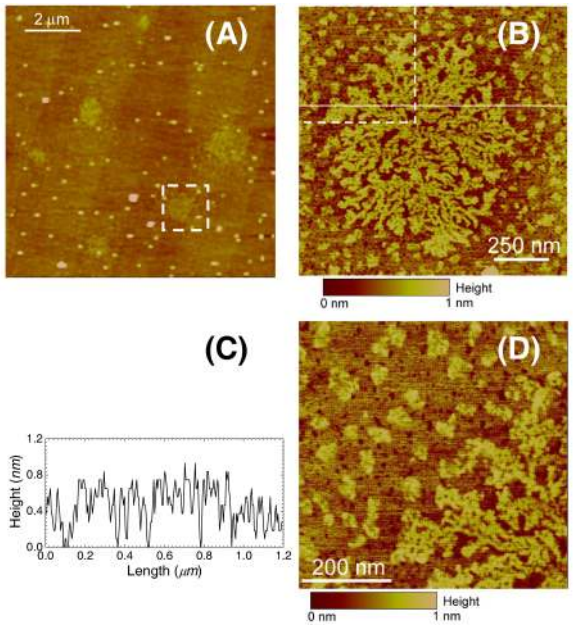

Fig. 5. (A) AFM height image of fractal aggregates of dendrimer **1** on mica. (B) Aggregate of dendrimer **1** from the area indicated in (A). Fractal dimension $D = 1.80$. (C) Profile of the line shown in (B). (D) Magnified image of part of the fractal structure and smaller aggregates from the area indicated in (B).

the island until they stick, so that a large-scale, continuous film develops.

The formation of films of dendrimer **1** that are less than 1 nm thick is consistent with observations of other dendrimers. The hydrodynamic diameters of the parent DAB-dendr-$(NH_2)_8$ in N,N-dimethylacetamide from small-angle X-ray scattering and small-angle neutron scattering data are 1.46 nm and 1.24 nm, respectively [40–42]. Although higher-generation dendrimers are globular due to crowded chain ends, lower-generation dendrimers such as **1** are not crowded and have an average oblate ellipsoidal geometry [25,36,43,44]. Even PPI dendrimers having 64 hexadecanoyl end groups assume flat conformations on a water surface [45]. Poly(amido amine) (PAMAM) dendrimers also tend to flatten when adsorbed to a surface or spread at an air-water interface [46–49]. Molecular dynamics and Monte Carlo calculations indicate that PPI and PAMAM dendrimers can assume flat conformations [50,51]. Dendrimers also form patterned surfaces when deposited as an aerosol [52].

The noncovalent self-assembly of dendrimers into three-dimensional aggregates is due to hydrogen bonding and van der Waals forces and is controlled by anisotropic molecular shape and amphiphilic character. Molecular dynamics simulation shows that the parent DAB-dendr-$(NH_2)_8$ has nearly two-dimensional shape with relative shape anisotropy of 0.22 and a fractal dimension of 2.56 [25]. Dynamic light scattering measurement of dendrimer **1** in chloroform gave a hydrodynamic diameter of 0.8 nm, which is too small to be true and too small to measure reliably with our instrument, but does indicate that the dendrimer dissolves molecularly. The aggregates of dendrimer **1** shown in Figure 4 are two dimensional, having thicknesses of ≤ 0.8 nm. Previous theoretical and experimental studies have shown that dendrimers adsorbed to a surface resemble flat disks [50,53]. Since 0.8 nm is less than the thickness of two aliphatic hydrocarbon chains, the $C_{11}H_{23}$ chains of the dendrimer must lie essentially parallel to the mica surface.

To observe in further detail the growth of the domains of the hydrophobically modified dendrimer and to further understand the role of kinetics, we spin-coated dendrimer **1** onto mica from a 2.0 mg mL^{-1} solution in chloroform. AFM images of the resulting film, shown in Figure 5, have fractal patterns. At the lower magnification in Figure 5A there are fractal aggregates $> 1\,\mu$m in diameter. The magnified images in Figures 5B and D show that the fractal structure consists of smaller aggregates, and that many of the smaller aggregates also are present on the mica surface. From the section analysis of Figure 5C, the typical height of the dendrimer fractal aggregates is 0.6–0.8 nm. Thus the fractal aggregates are flat, nearly two-dimensional films. The surface irregularity and anisotropy of the PPI dendrimer lower its sticking probability. This allows the dendrimer particles to explore more of the existing fractal structure before attaching, and allows particles to attach to the perimeter of the fractal.

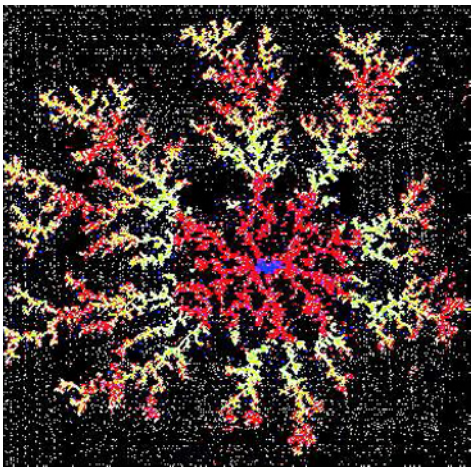

Fig. 6. (Colour online) A fractal of dendrimers grown by diffusion-limited dendrimer-cluster aggregation on a square lattice using a fractal generator. The colors show different stages of fractal evolution.

The difference between the fractal aggregates and the disk-shaped aggregates arises from the kinetics of the adsorption process. After 30 s for diffusion in chloroform solution and adsorption to both the existing adsorbed dendrimer and the mica surface, the dendrimer packed into the 0.8 nm high disk-shaped aggregates shown in Figure 4. In contrast, when aggregate growth was stopped by rapidly spinning away the excess solution in 20 seconds for adsorption, the aggregates were the 0.6–0.8 nm high fractal shown in Figure 5. Thus diffusion-limited aggregation to fractals occurs first, and the void spaces in the fractals fill in over longer time.

Formation of the fractal structure was simulated using the fractal generator, MicroMod [54]. We added 9000 dendrimer particles to a single seed on a 500×500 square lattice using multi-step random trajectories and a sticking probability of 0.3. The resulting cluster shown in Figure 6 has a fractal dimension of 1.7. The similarity of Figure 5B and Figure 6 suggests that the fractal aggregate was formed on the mica through a diffusion-limited aggregation (DLA) process [55,56].

The fractal nature of the image in Figure 5B was confirmed by calculating its fractal dimension, D. Using a scaling rule, the fractal dimension is calculated from the ratio of the log of the number of new objects, N, to the log of the object size, r:

$$D = \lim_{r \to 0} \left[\frac{\log N}{\log r} \right].$$

We first converted the color-coded AFM images to binary using the digital image editing program, ImageJ [57]. A threshold criterion was applied to separate pixels in the cluster from those in the background. Using the fractal image analysis program, FracLac [58], we found the fractal dimension from the slope of the regression line of the logarithmic plot of the number of such cluster pixels (N) *versus* the size of the cluster (r). For the AFM image of

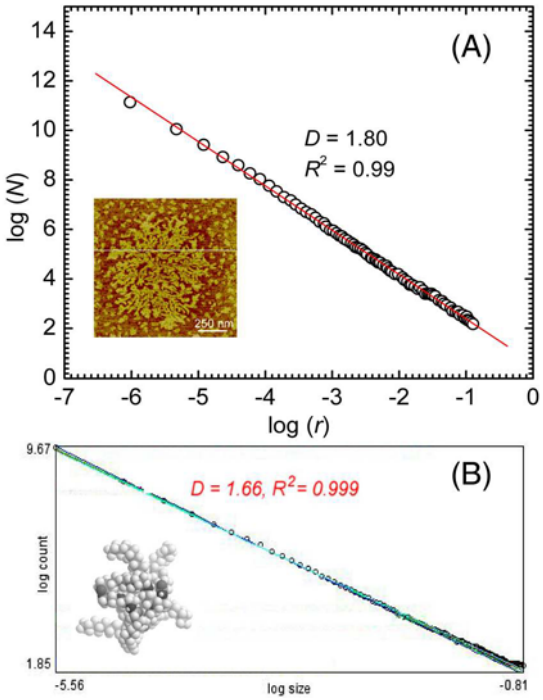

Fig. 7. Log-log graphs of N *versus* r based on the box-counting method for both the experimental $2D$ dendrimer aggregate (A) and the MM2 structure of the hydrophobically modified dendrimer molecule (B). Here, N is the number of boxes in each box-grid that contains part of the structure and r is the unit size of boxes across the bottom of the grid. The fractal dimension, D, is the absolute value of the slope.

the fractal aggregates on mica, the graph of $\log(N)$ *versus* $\log(r)$ yielded a fractal dimension D of 1.80 from the slope of the straight line with an R^2 value of 0.99, as shown in Figure 7. This corresponds to aggregates formed by diffusion-limited aggregation (DLA) [26,55,56,59,60].

In summary, spin-coating of the hydrophobically modified PPI dendrimer **1** forms aggregates on a mica surface with a fractal dimension of 1.80. The presence of smaller clusters similar to the clusters comprising the fractal aggregates and modeling of fractal growth suggest that the fractal was formed by a cluster-cluster diffusion-limited aggregation process. The height of the fractal film was no more than 0.8 nm, which requires dendrimer conformations in which the inner segments, branch points, and peripheral aliphatic chains all lie roughly parallel to the surface of the mica.

3.2 Flow of fractal aggregates

Diffusion-limited aggregation means that the fractal structures form under kinetically controlled conditions. Since the glass transition temperature of the PPI core [DAB-dendr-$(NH_2)_8$] of dendrimer **1** is −65 °C [61], and C12 chains in monolayers and bilayers do not crystallize at room temperature, the dendrimer film on mica should anneal at room temperature. Figure 8 shows images of 5-month-old samples. The aggregates now appear as disks

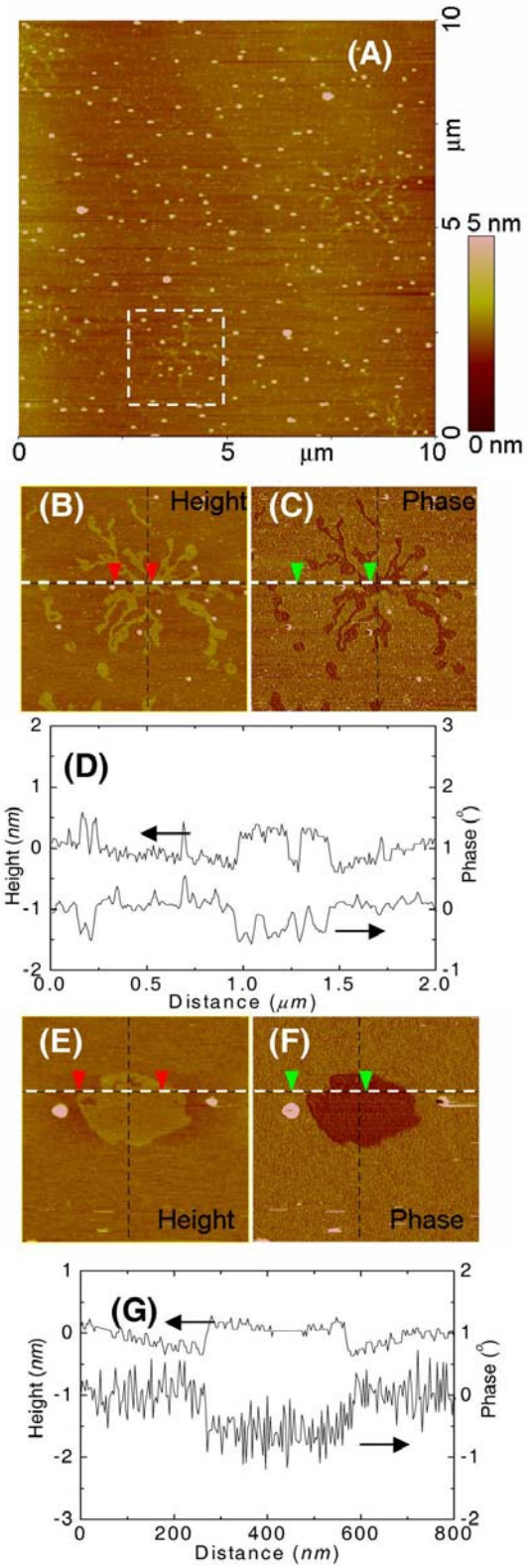

Fig. 8. AFM images (A, B, C, E, and F) of the fractal aggregates after 5 months in air at 25 °C and line profiles (D and G) across the aggregates. The small light spots in height image A are attributed to dust and not dendrimer because they contrast strongly with the dendrimer in the phase image C. B and C are 2 μm × 2 μm images of one fractal aggregate of A. E and F are 800 nm × 800 nm images of one disk-shaped aggregate.

and the fractals have lost all but their main branches. The average heights of the disks and collapsed fractals are 0.6 nm and 0.4 nm, respectively, which are less than the 0.8 nm observed earlier for the fractal aggregates. Thus the dendrimer aggregates on mica flow slowly over a time scale of months, whereas adsorption from a chloroform solution to fill in the void spaces of the fractals of Figure 5 and give the disks of Figure 4 takes place in tens of seconds. The thermodynamically stable form of the film, which has not been reached in Figure 8, is likely a monolayer of thickness < 0.8 nm.

4 Conclusions

Depositions of dendrimer **1** from solution onto mica by adsorption to form less than a full monolayer are kinetic processes controlled by diffusion and attractive interactions between dendrimer molecules and between dendrimer and mica. With sufficient time of adsorption, the hydrophobically modified dendrimer **1** forms continuous films on mica. Islands and fractal aggregates form by adsorption over shorter time. The presence of smaller clusters similar to the clusters comprising the fractal aggregates and modeling of fractal growth suggest that the fractal was formed by a cluster-cluster diffusion-limited aggregation process. The height of the fractal film was no more than 0.8 nm, which requires dendrimer conformations in which the inner segments, branch points, and peripheral aliphatic chains all lie roughly parallel to the surface of the mica. Annealing of the initial fractal aggregates at room temperature led to merging of small branches into the interior of the hollow aggregates, leaving shapes in which the fractals have lost all but their main branches.

Acknowledgments are made to the National Science Foundation (grant EPS-0132354) and the Donors of the American Chemical Society Petroleum Research Fund for support of this research.

References

1. G.R. Newkome, C.N. Moorefield, F. Vögtle, *Dendrimers and Dendrons: Concepts, Synthesis, Applications* (Wiley-VCH Verlag, Weinheim, 2001).
2. D.A. Tomalia, Mater. Today **8**, 34 (2005).
3. J. Wang, Y. Cheng, T. Xu, Recent Patents Chem. Eng. **1**, 41 (2008).
4. K.T. Al-Jamal, C. Ramaswamy, A.T. Florence, Adv. Drug Delivery Rev. **57**, 2238 (2005).
5. M. Marcos, A. Martín-Rapún, A. Omenat, J.L. Serrano, Chem. Soc. Rev. **36**, 1889 (2007).
6. S.S. Sheiko, A.M. Muzafarov, R.G. Winkler, E.V. Getmanova, G. Eckert, P. Reineker, Langmuir **13**, 4172 (1997).
7. D.C. Tully, J.M.J. Frechet, Chem. Commun. 1229 (2001).
8. S.C. Zimmerman, L.J. Lawless, Top. Curr. Chem. **217**, 95 (2001).

9. A. Su, S. Tan, P. Thapa, B.N. Flanders, W.T. Ford, J. Phys. Chem. C **111**, 4695 (2007).
10. J.-W. Weener, E.W. Meijer, Adv. Mater. **12**, 741 (2000).
11. A. Schenning, C. Elissen-Roman, J.W. Weener, M. Baars, S.J. van der Gaast, E.W. Meijer, J. Am. Chem. Soc. **120**, 8199 (1998).
12. P.M. Saville, P.A. Reynolds, J.W. White, C.J. Hawker, J.M.J. Frechet, K.L. Wooley, J. Penfold, J.R.P. Webster, J. Phys. Chem. **99**, 8283 (1995).
13. P.M. Saville, J.W. White, C.J. Hawker, K.L. Wooley, J.M.J. Frechet, J. Phys. Chem. **97**, 293 (1993).
14. Y. SayedSweet, D.M. Hedstrand, R. Spindler, D.A. Tomalia, J. Mater. Chem. **7**, 1199 (1997).
15. J.P. Kampf, C.W. Frank, E.E. Malmstrom, C.J. Hawker, Langmuir **15**, 227 (1999).
16. M. Ujihara, J. Orbulescu, T. Imae, R.M. Leblanc, Langmuir **21**, 6846 (2005).
17. X. Zhai, S. Peleshanko, N.S. Klimenko, K.L. Genson, D. Vaknin, M.Y. Vortman, V.V. Shevchenko, V.V. Tsukruk, Macromolecules **36**, 3101 (2003).
18. K.L. Genson, J. Holzmuller, O.F. Villacencio, D.V. McGrath, D. Vaknin, V.V. Tsukruk, J. Phys. Chem. B **109**, 20393 (2005).
19. K.L. Genson, D. Vaknin, O. Villacencio, D.V. McGrath, V.V. Tsukruk, J. Phys. Chem. B **106**, 11277 (2002).
20. R. Gunawidjaja, S. Peleshanko, K.L. Genson, C. Tsitsilianis, V.V. Tsukruk, Langmuir **22**, 6168 (2006).
21. R.N. Mason, M. Smith, T. Andrews, D. Teeters, Solid State Ionics **118**, 129 (1999).
22. F.I. Li, S.M. Thaler, P.H. Leo, J.A. Barnard, J. Phys. Chem. B **110**, 25838 (2006).
23. ChemOffice by CambridgeSoft Corporation (`http://www.cambridgesoft.com/software/ChemOffice/`) was used to minimize the molecular energy.
24. D.N. Theodorou, U.W. Suter, Macromolecules **18**, 1206 (1985).
25. N. Zacharopoulos, L.G. Economou, Macromolecules **35**, 1814 (2002).
26. W.T. Elam, S.A. Wolf, J. Sprague, D.U. Gubser, D. Vanvechten, G.L. Barz, P. Meakin, Phys. Rev. Lett. **54**, 701 (1985).
27. D.T. Smith, J.J.M. Valles, R.B. Hallock, Phys. Rev. Lett. **54**, 2646 (1985).
28. M. Fujii, K. Arii, K. Yoshino, J. Phys.: Condens. Matter **3**, 7207 (1991).
29. Q. Wu, L. Wu, Z. Qi, F. Wang, Synth. Met. **105**, 13 (1999).
30. D.K. Schwartz, S. Steinberg, J. Israelachvili, J.A.N. Zasadzinski, Phys. Rev. Lett. **69**, 3354 (1992).
31. A. Lomander, W. Hwang, S. Zhang, Nano Lett. **5**, 1255 (2005).
32. R. Sneer, M.J. Weygand, K. Kjaer, D.A. Tirrell, H. Rapapport, ChemPhysChem **5**, 747 (2004).
33. S. Tan, D. Zhang, E. Zhou, Polymer **38**, 4571 (1997).
34. R.P. Wool, J.M. Long, Macromolecules **26**, 5227 (1993).
35. D. Farin, D. Avnir, Angew. Chem. Int. Ed. **30**, 1379 (1991).
36. D.A. Tomalia, A.M. Naylor, W.A. Goddard III, Angew. Chem. Int. Ed. **29**, 138 (1990).
37. Y. Pan, W.T. Ford, Macromolecules **33**, 3731 (2000).
38. T.P. Bigioni, X.-M. Lin, T.T. Nguyen, E.I. Corwin, T.A. Witten, H.M. Jaeger, Nature Mater. **5**, 265 (2006).
39. A. Flores, E. Corvera-Poire, C. Garza, R. Castillo, J. Phys. Chem. B **110**, 4824 (2006).
40. T.J. Prosa, B.J. Bauer, E.J. Amis, D.A. Tomalia, R. Scherrenberg, J. Polym. Sci. Polym. Phys. **35**, 2913 (1997).
41. R. Scherrenberg, B. Coussens, P. van Vliet, G. Edouard, J. Brackman, E. de Brabander, K. Mortensen, Macromolecules **31**, 456 (1998).
42. A. Ramzi, B.J. Bauer, R. Scherrenberg, P. Froehling, J. Joosten, E.J. Amis, Macromolecules **32**, 4983 (1999).
43. P. Brocorens, R. Lazzaroni, J.L. Bredas, J. Phys. Chem. B **109**, 19897 (2005).
44. M.L. Mansfield, L.I. Klushin, Macromolecules **26**, 4262 (1993).
45. A.P.H.J. Schenning, C. Elissen-Roman, J.-W. Weener, M.W.P.L. Baars, S.J. van der Gaast, E.W. Meijer, J. Am. Chem. Soc. **120**, 8199 (1998).
46. H. Tokuhisa, M.Q. Zhao, L.A. Baker, V.T. Phan, D.L. Dermody, M.E. Garcia, R.F. Peez, R.M. Crooks, T.M. Mayer, J. Am. Chem. Soc. **120**, 4492 (1998).
47. K.L. Genson, J. Holzmueller, I. Leshchiner, E. Agina, N. Boiko, V.P. Shibaev, V.V. Tsukruk, Macromolecules **38**, 8028 (2005).
48. V.V. Tsukruk, Adv. Mater. **10**, 253 (1998).
49. K. Tanaka, S. Dai, T. Kajiyama, K. Aoi, M. Okada, Langmuir **19**, 1196 (2003).
50. A. Mecke, I. Lee, J.R. Baker Jr., M.M.B. Holl, B.G. Orr, Eur. Phys. J. E **14**, 7 (2004).
51. G. Giupponi, D.M.A. Buzza, J. Chem. Phys. **122**, 194903 (2005).
52. F.T. Xu, S.C. Street, J.A. Barnard, Langmuir **19**, 3066 (2003).
53. M.L. Mansfield, Polymer **37**, 3835 (1996).
54. A. Karperien (`http://rsb.info.nih.gov/ij/plugins/fractal-generator.html`). Accessed August 15, 2005.
55. T.A. Witten, L.M. Sander, Phys. Rev. Lett. **47**, 1400 (1981).
56. T.A. Witten, L.M. Sander, Phys. Rev. B **27**, 5686 (1983).
57. National Institutes of Health. (`http://rsb.info.nih.gov/ij`). Accessed August 15, 2005.
58. A. Karperien (`http://rsb.info.nih.gov/ij/plugins/frac-lac.html`). Accessed August 15, 2005.
59. A. Blumen, H. Schnorer, Angew. Chem. Int. Ed. **29**, 113 (1990).
60. R. Pericet-Camara, G. Papastavrou, M. Borkovec, Langmuir **20**, 3264 (2004).
61. E.M.M. de Brabander-van den Berg, E.W. Meijer, Angew. Chem. Int. Ed. **32**, 1308 (1993).